bioRxiv preprint doi: https://doi.org/10.1101/094631; this version posted December 15, 2016. The copyright holder for this preprint (which was not certified by peer review) is the author/funder, who has granted bioRxiv a license to display the preprint in perpetuity. It is made available under aCC-BY 4.0 International license.

Development of Narrow Spectrum ATP-competitive Kinase Inhibitors as Probes for BIKE and AAK1

Rafael M. Couñago[1], Alison D. Axtman[2], Hátylas Azevedo[3], David H. Drewry[2], Jonathan M. Elkins[1,4], Opher Gileadi[1,4], Cristiano R. W. Guimarães[3], Alessandra Mascarello[3], Carrow I. Wells[2], Timothy M. Willson[2], William J. Zuercher[2,*]

[1]Structural Genomics Consortium, Universidade Estadual de Campinas — UNICAMP, Campinas, SP, Brazil.
[2]Structural Genomics Consortium, UNC Eshelman School of Pharmacy, University of North Carolina at Chapel Hill, Chapel Hill, NC, USA.
[3]Aché Laboratórios Farmacêuticos SA, Guarulhos, SP, Brazil.
[4]Structural Genomics Consortium and Target Discovery Institute, Nuffield Department of Clinical Medicine, University of Oxford, Old Road Campus Research Building, Oxford, OX3 7DQ, UK.

*Correspondence to W. Zuercher, email: william.zuercher@unc.edu

ABSTRACT: Understanding the structural determinants of inhibitor selectivity would facilitate the design and preparation of kinase probes. We describe a pair of matched compounds differing only by one degree of saturation but showing dramatic differential activities at select kinases. We utilized x-ray crystallography and computational analysis to rationalize the basis of the differential activity.

INTRODUCTION

The human protein kinases are a family of over 500 enzymes that are involved in critical aspects of cell signaling but are often dysregulated in disease, especially cancer (Cohen and Alessi 2013). Protein kinases catalyze the transfer of phosphate from the cofactor ATP to their substrate proteins. Although ATP-competitive protein kinase inhibitors have been successfully developed to treat a range of cancers, inflammatory and fibrotic diseases, the function of a large number of the enzymes remains unknown (Fedorov, Muller et al. 2010). Potent and selective small molecule inhibitors are powerful tools to probe the biology of these understudied kinases (Uitdehaag, Verkaar et al. 2012).

Because ATP-competitive inhibitors bind to a common active site, they often show activity across multiple kinases. For example, staurosporine inhibits more than 200 protein kinases. These broad spectrum inhibitors are useful for initial biochemical characterization but have little utility as probes of kinase biology (Ruegg and Burgess 1989). By contrast, other ATP-competitive inhibitors possess activity on only a handful of kinases. These narrow spectrum inhibitors have found utility in exploring the function of several historically understudied kinases (Knapp, Arruda et al. 2013).

To strengthen the conclusions drawn from use of narrow spectrum kinase inhibitors, a recently established best practice is to use the probe molecule in parallel with a

bioRxiv preprint doi: https://doi.org/10.1101/094631; this version posted December 15, 2016. The copyright holder for this preprint (which was not certified by peer review) is the author/funder, who has granted bioRxiv a license to display the preprint in perpetuity. It is made available under aCC-BY 4.0 International license.

negative control, a closely-related analogue that is inactive for the target kinase (Arrowsmith, Audia et al. 2015). Demonstration of divergent results between the probe inhibitor and its negative control increases confidence that the engagement of the target kinase was responsible for the observed biology.

For ATP-competitive kinase inhibitors, a systematic approach to develop negative control analogs is to synthesize a molecule that lacks the ability to form the critical hinge binding interaction, typically composed of one or more hydrogen bonds with the highly conserved hinge region in the enzyme (Xing, Klug-Mcleod et al. 2015). These modifications result in "kinase dead" analogues. Unfortunately, kinase dead analogues often lose affinity not only for the primary target kinase but also for all other off-target kinases. New strategies to create kinase probe negative controls that lose affinity selectively for their target kinase are needed.

Here we describe a pair of compounds in which a minor structural change—namely, the inclusion of a cyclopropyl versus an isopropyl substituent proximal to the hinge-binding moiety—leads to unexpectedly large changes in activity within a small subset of protein kinases but no change against many others. We used X-ray crystallography and computational models to study the molecular basis for these differential effects on affinity within the target and off-target kinases in an attempt to define general approaches to design selective negative control analogs.

RESULTS

As part of a large-scale selectivity screen of ATP-mimetic kinase inhibitors, we identified a pair of very closely related 3-acylaminoindazoles (**1** and **2**) that displayed a narrow binding spectrum in the KINOMEscan panel of over 400 human protein kinase assays at an inhibitor concentration of 1 µM (**Supplementary Table 1**). Structurally, **1** and **2** differed only by the addition of two hydrogen atoms in the change from a cyclopropyl to isopropyl carboxamide. **1** and **2** had many common kinase targets but also showed some degree of divergence in kinase affinity profiles. A more detailed analysis of their binding characteristics revealed that **1** had submicromolar affinity for 11 kinases and weaker affinity for 2 additional kinases (**Table 1)**, while **2** showed submicromolar affinity for 7/11 of the primary kinases targets and 1/2 of the minor targets. For most of the target kinases, only marginal differences in potency were observed between the analogs (<3-fold). However, four kinases (AAK1, BIKE, RIOK1, and RIOK3) displayed remarkable differential affinity between the cyclopropyl analog **1** and isopropyl analog **2** with a preference for the former (27–150-fold).

AAK1 and BIKE, along with the related GAK and STK16, comprise the Numb-associated kinase (NAK) subfamily of protein kinases (Sorrell, Szklarz et al. 2016). NAK family members have been proposed as potential drug targets for a wide range of therapeutic areas, including virology, oncology, neurology, and ophthalmology (Liu, Lin et al. 2009, Sakurai, Ozaki et al. 2014, Shi, Conner et al. 2014, Neveu, Ziv-Av et al. 2015). In contrast, relatively little is known about the relevance to cellular processes of the atypical kinases

bioRxiv preprint doi: https://doi.org/10.1101/094631; this version posted December 15, 2016. The copyright holder for this preprint (which was not certified by peer review) is the author/funder, who has granted bioRxiv a license to display the preprint in perpetuity. It is made available under aCC-BY 4.0 International license.

RIOK1 and RIOK3. Accordingly, to explore the molecular basis of the remarkable differential activities of **1** and **2**, we decided to study their interaction with the NAK family kinases. **1** and **2** were evaluated in FRET-based binding displacement assays (Lebakken, Riddle et al. 2009). The cyclopropyl analog **1** showed >300-fold increased affinity for AAK1 and BIKE relative to the isopropyl analog **2** (**Table 2**). Both compounds demonstrated weaker affinity for GAK and STK16, although a >50-fold preference for **1** relative to **2** was also observed with the latter kinase.

*Structural analysis of compound **1** binding***.** BIKE and AAK1 are the closest members within the NAK family and share a high sequence identity—74% over their kinase domains and 81% within their ATP-binding sites. In order to obtain insights into the molecular details of ligand interactions with these kinases, we determined the cocrystal structure of BIKE kinase domain bound to compound **1** (**Table 3**), reasoning that both kinases are likely to interact with **1** and **2** in similar manners.

BIKE-**1** crystals diffracted to 2.4 Å, and displayed a single protein chain per asymmetric unit (chain A). Sorrell and colleagues have recently reported the structural characterization of all four NAK family member kinase domains, including BIKE and AAK1 (Sorrell, Szklarz et al. 2016). As previously observed, our structure of BIKE displayed a catalytically-competent conformation in which residues in the protein regulatory spine ("R spine"; residues M99, Y111, H178 and F199) are aligned and side-chain atoms from conserved residues in β3 and α-C (K79 and E95, respectively) form an ion pair (Huse and Kuriyan 2002, Kornev and Taylor 2010). Moreover, the NAK family-exclusive helical domain (P209 to Y224) found C-terminal of the activation segment (from ^{198}DFG to APE^{233} domains), dubbed ASCH (activation segment C-terminal helix) (Eswaran, Bernad et al. 2008, Chaikuad, Keates et al. 2014, Sorrell, Szklarz et al. 2016), also displayed an identical conformation in the BIKE structure described here (**Figure 1a**).

The cocrystal structure of **1** and BIKE reveals that 3-acylaminoindazole **1** is anchored to the protein hinge region (BIKE residues 131-137) *via* hydrogen bonds between the N atoms of the indazole group and main chain carbonyl and NH groups of residues Glu131 and Cys133, respectively. An additional hydrogen bond is made between the amino group of **1** and the carbonyl group of Cys133. At the other end of the inhibitor, the sulfonamide group engages residues Gln137 and Asn185 via hydrogen bonds. These interactions position the pendant aliphatic group into a hydrophobic cavity within the P-loop formed by residues Val65 and Ser65. The indazole and the aniline rings are not co-planar to each other. This flexibility provides excellent shape-complementarity between the inhibitor and the ATP-binding pocket; especially with the aliphatic side chains from Leu187 and from p-loop residues Leu57, Ala58 and Val65. There is also a sulfur-π interaction between the aniline ring and the sulfur atom of Cys197 (**Figure 1b**). Residue Cys197 is adjacent to the protein DFG motif and has been proposed as a site of covalent modification by the inhibitor (5*Z*)-7-oxozeaenol (Sorrell, Szklarz et al. 2016). The cyclopropane group adjacent to the carboxyl group in **1** is accommodated within a sharp turn of the peptide backbone involving residues occupying positions +3, +4 and +5 from

bioRxiv preprint doi: https://doi.org/10.1101/094631; this version posted December 15, 2016. The copyright holder for this preprint (which was not certified by peer review) is the author/funder, who has granted bioRxiv a license to display the preprint in perpetuity. It is made available under aCC-BY 4.0 International license.

the so-called gatekeeper, or GK, residue (Met130 in BIKE). This kink in the peptide backbone allows the carbonyl groups of residues GK+3 (Cys133) and GK+4 (Arg134) to point towards the cyclopropyl C-H group, approaching at a distance of 3.6 and 3.3 Å, respectively (**Figure 1b**).

We compared our BIKE-**1** structure with published structures of DDR1 (PDB: 5FDP), BRAF (PDB: 4XV9), AAK1 (PDB: 4WSQ), and RIOK1 (PDB: 4OTP) to attempt to rationalize the structural basis differential activity of **1** and **2** on some but not all kinases. Surface electrostatic potential is quite different for kinases that show differential activity compared with those that do not. AAK1, BIKE, and RIOK1 have bland surface charge where the critical cyclopropyl moiety of **1** is accommodated within the binding pocket. In contrast, BRAF and DDR1 have highly charged surfaces around their corresponding hinge binding regions.

Superimposing our BIKE-**1** structure with the previously published structures from the NAK family (Sorrell, Szklarz et al. 2016) by aligning the hinge residues (rmsd < 0.3 Å for 7 equivalent Cα) revealed that the P-loop of STK16 and GAK are substantially displaced compared to the position occupied by this region in BIKE and AAK1 structures (**Figure 1d**). The extensive contacts **1** makes with the P-loop may explain its selectivity for BIKE and AAK1 over the other two members of the NAK family. Interestingly, the primary sequence alignment of NAK family members reveals that sequence conservation is high for the P-loop region and low for the hinge moiety (**Figure 1e**).

Computational studies. A range of computational methodologies was applied to shed light on the differential affinities of **1** and **2**. Energy minimization calculations in the unbound state using the OPLS3 force field (Harder, Damm et al. 2016) and the GB/SA (Still, Tempczyk et al. 1990) solvation model suggest that dehydration penalty upon binding is not a dominant factor, as similar hydration values were obtained for **1** (-29.8 kcal/mol) versus **2** (-29.2 kcal/mol); the cyclopropyl analog was actually slightly more penalized. To investigate the electronic properties, electrostatic potential derived atomic charges using the B3LYP exchange-correlation energy functional (Stephens, Devlin et al. 1994) and the 6-31G** basis set (Frisch, Pople et al. 1984) were obtained in the gas phase. In this case, striking differences were observed for the C-H bond adjacent to the carbonyl group; it was much more polarized for cyclopropyl than isopropyl (**Figure 2**), with no major differences for the adjacent amide.

DISCUSSION

3-Acylaminoindazoles are a known class of ATP-competitive protein kinase inhibitors (Witherington, Bordas et al. 2003). The heterocyclic core mimics the adenosine base of ATP and forms hydrogen bonds with the hinge motif of the enzyme. We have described a pair of closely-related cyclopropyl and isopropyl 3-acylaminoindazoles, **1** and **2**, differing by only two hydrogen atoms. Screening across 400 human protein kinases revealed both compounds to be narrow spectrum inhibitors, with high affinity binding to <3% of the kinases surveyed. Both **1** and **2** bound to seven kinases (ABL1, BRAF,

bioRxiv preprint doi: https://doi.org/10.1101/094631; this version posted December 15, 2016. The copyright holder for this preprint (which was not certified by peer review) is the author/funder, who has granted bioRxiv a license to display the preprint in perpetuity. It is made available under aCC-BY 4.0 International license.

DDR1, KIT, PDGFRA, PDGFRB, and RAF1) with submicromolar affinity. Surprisingly, cyclopropyl amide **1** bound to an additional four kinases (AAK1, BIKE, RIOK1, and RIOK3) where isopropyl amide **2** was not effective. Thus, this pair of ATP-competitive kinase inhibitors have the potential to be used to probe selectively the biology of just 4 protein kinases while controlling for over 400 others in the human genome.

BIKE and AAK1 are both members of the NAK (Numb-associated kinase) family of protein kinases and share close sequence identity within their catalytic sites. Both kinases are potently inhibited by the 3-acylaminoindazoles **1** and are likely to interact with the inhibitor through conserved interactions. The BIKE-**1** cocrystal structure provides a clear view into the molecular details of the enzyme-ligand interaction. The critical cyclopropyl carboxamide sits in a pocket adjacent to the hinge-binding residues and is orientated toward protein surface. The amide NH of **1** and the cyclopropyl ring C-H sit in close proximity (2.7 and 3.29 Å, respectively) to the Cys133 carbonyl oxygen (**Figure 3**). Our *ab initio* calculations showed that the cyclopropyl group has an increased polarization across the ring C-H compared the corresponding isopropyl analogue. The complex between the cyclopropyl derivative **1** and BIKE is indicative of a CH-O nonconventional hydrogen bond. Electrostatic interactions dominate hydrogen bonds and the increased polarization of the cyclopropyl C-H bond, as evidenced by the electrostatic potential charges, may explain why **1** shows significantly higher affinity for AAK1/BIKE than the isopropyl analog **2**.

The term "activity cliff" has been proposed to describe pairs of structurally similar compounds, like **1** and **2**, with a large difference in potency relative to a common target (Stumpfe and Bajorath 2012). There have been other reports of kinase inhibitor activity cliffs involving cyclopropyl and isopropyl carboxamides proximal to their hinge binding moiety (**Table 4**). The 2-cyclopropylcarboxamidopyridine **3a** showed >100x higher affinity for TYK2 than the isopropyl analog **3b** (Liang, Tsui et al. 2013). Similarly, **4a** displayed a much high inhibition potency than **4b** in a biochemical assay of mutant B-Raf^{V600E} activity (Li, Shen et al. 2016). These examples substantiate our observations that subtle changes in C-H bond polarization can lead to selective inhibition of specific protein kinases. Further, by subjecting **1** and **2** to kinome-wide profiling, we have defined the breadth of the activity cliff, showing that it is maintained across only a narrow subset of kinases.

The cyclopropyl ring is a versatile lipophilic group that frequently appears in preclinical and clinical candidate molecules. It has been described to have "magical" properties; it can enhance potency, reduce off-target effects, increase metabolic stability and brain permeability, yet the precise molecular basis for these effects are not clearly understood (Talele 2016). Theoretical studies on cyclopropane and its derivatives suggest that atomic bonding results mainly from the overlap of three sp^2 hybrids (one on each carbon) pointing towards the center of the ring. Thus, the electron distribution in the C-C internuclear region is not concentrated along the line between the nuclei, but rather slightly outside this line. As a consequence, the C-C bonds have enhanced π

bioRxiv preprint doi: https://doi.org/10.1101/094631; this version posted December 15, 2016. The copyright holder for this preprint (which was not certified by peer review) is the author/funder, who has granted bioRxiv a license to display the preprint in perpetuity. It is made available under aCC-BY 4.0 International license.

character and the C-H bonds have more *s* character. In other words, the cyclopropyl ring behaves much like an alkene, interacts with neighboring π-electron systems, and its CH bonds are more acidic (Galano, Alvarez-Idaboy et al. 2007). These effects are apparent when the emerging negative charge on the C-H carbon is stabilized by conjugation, such as the one between the π-like cyclopropyl and an amide carbonyl group. These effects are revealed in the calculated electrostatic potential charges, as demonstrated above.

Comparison with other published x-ray structures of kinases suggested that electrostatic surface potential near the hinge binding region might be important in determining whether a specific kinase can discriminate between **1** and **2**. However, this analysis was conducted on a limited number of crystal structures, each bound to a different inhibitor. We recognize that there are myriad other subtle changes in the binding pockets that must also be explored to enable prediction of which kinases can be differentially inhibited by matched ligand pairs. However, our enhanced understanding of how the cyclopropyl group of **1** interacts within the AAK1 and BIKE binding pockets will improve our ability to produce narrow spectrum probes with optimal negative control analogs for use in biological studies.

MATERIALS AND METHODS

N-(6-(3-(cyclopropanesulfonamido)phenyl)-1*H*-indazol-3-yl)cyclopropanecarboxamide (**1**). ^{1}H NMR (400 MHz, Methanol-d_4) δ 7.83 – 7.78 (d, *J* = 8.6 Hz, 1H), 7.61 – 7.54 (m, 2H), 7.46 – 7.30 (m, 3H), 7.29 – 7.23 (ddd, *J* = 7.7, 2.2, 1.3 Hz, 1H), 2.62 – 2.49 (tt, *J* = 8.0, 4.8 Hz, 1H), 1.95 – 1.84 (ddd, *J* = 12.5, 7.9, 4.2 Hz, 1H), 1.07 – 0.77 (m, 8H). MS+ (– ES API) - 397.1

N-(6-(3-(cyclopropanesulfonamido)phenyl)-1*H*-indazol-3-yl)isobutyramide (**2**). ^{1}H NMR (400 MHz, Methanol-d_4) δ 7.82 – 7.75 (d, *J* = 8.6 Hz, 1H), 7.62 – 7.54 (dt, *J* = 10.9, 1.5 Hz, 2H), 7.47 – 7.31 (m, 3H), 7.31 – 7.22 (ddd, *J* = 7.8, 2.2, 1.3 Hz, 1H), 2.84 – 2.69 (hept, *J* = 6.8 Hz, 1H), 2.61 – 2.50 (tt, *J* = 8.0, 4.8 Hz, 1H), 1.29 – 1.15 (d, *J* = 6.8 Hz, 6H), 1.14 – 0.82 (m, 4H). MS+ (– ES API) - 399.1

DiscoverX kinase affinity measurements. KINOMEscan assay panel profiling and associated K_d determinations were obtained at DiscoverX Corporation using their previously described methodology (Fabian, Biggs et al. 2005, Davis, Hunt et al. 2011).

Binding displacement assays. Inhibitor binding was determined using a binding-displacement assay, which tests the ability of the inhibitors to displace a fluorescent tracer compound from the ATP binding site of the kinase domain. Inhibitors were dissolved in DMSO and dispensed as 16-point, 2x serial dilutions in duplicate into black multiwell plates (Greiner). Each well contained either 0.5 nM or 1 nM biotinylated kinase domain protein ligated to streptavidin-Tb-cryptate (Cisbio), 12.5 nM or 25 nM Kinase Tracer 236 (ThermoFisher Scientific), 10 mM Hepes pH 7.5, 150 mM NaCl, 2 mM DTT, 0.01% BSA, 0.01% Tween-20. Final assay volume for each data point was 5 µL, and final DMSO concentration was 1%. The plate was incubated at room temperature for 1.5

bioRxiv preprint doi: https://doi.org/10.1101/094631; this version posted December 15, 2016. The copyright holder for this preprint (which was not certified by peer review) is the author/funder, who has granted bioRxiv a license to display the preprint in perpetuity. It is made available under aCC-BY 4.0 International license.

hours and then read using a TR-FRET protocol on a PheraStarFS plate reader (BMG Labtech). The data was normalized to 0% and 100% inhibition control values and fitted to a four parameter dose-response binding curve in GraphPad Software. The determined IC_{50} values were converted to K_i values using the Cheng-Prusoff equation and the concentration and K_D values for the tracer (previously determined).

Cloning, Expression, Purification and crystallization. $BIKE_{38\text{-}345\ (K320A,\ K321A)}$ with a tobacco etch virus (TEV) protease cleavable, N-terminal 6xHis tag was expressed from vector pNIC-ZB. To improve BIKE crystallization, a cluster of surface entropy reduction mutations (Derewenda 2004) was engineered into the expression construct, K320A/K321A (Sorrell, Szklarz et al. 2016). For protein production, the host *E. coli* strain, BL21(DE3)-R3 expressing lambda phosphatase, was cultivated in TB medium (+ 50 µg/ml kanamycin, 35 µg/ml chloramphenicol) at 37°C until OD_{600} reached ~3 and then cooled to 18°C for 1 hour. Isopropyl 1-thio-D-galactopyranoside was added to 0.1 mM, and growth continued at 18°C overnight. The cells were collected by centrifugation then resuspended in 2x lysis buffer (100 mM HEPES buffer, pH 7.5, 1.0 M NaCl, 20 mM imidazole, 1.0 mM tris(2-carboxyethyl)phosphine, 2x Protease Inhibitors Cocktail Set VII (Calbiochem, 1/1000 dilution) and flash-frozen in liquid nitrogen. Cells were lysed by sonication on ice. The resulting proteins were purified using Ni-Sepharose resin (GE Healthcare) and eluted stepwise in binding buffer with 300 mM imidazole. Removal of the hexahistidine tag was performed at 4°C overnight using recombinant TEV protease. Proteins were further purified using reverse affinity chromatography on Ni-Sepharose followed by gel filtration (Superdex 200 16/60, GE Healthcare). Protein in gel filtration buffer (25 mM HEPES, 500 mM NaCl, 0.5 mM TCEP, 5% [v/v] glycerol) was concentrated to 12 mg/ml using 30 kDa MWCO centrifugal concentrators (Millipore) at 4°C. 3-acylaminoindazole **1** in 100% DMSO was added to the protein in a 3-fold molar excess and incubated on ice for approximately 30 minutes. The mixture was centrifuged at 14,000 rpm for 10 minutes at 4°C prior to setting up 150 nL volume sitting drops at three ratios (2:1, 1:1, or 1:2 protein-inhibitor complex to reservoir solution). Crystallization experiments were performed at 20°C. Crystals were cryoprotected in mother liquor supplemented with 2025% glycerol before flash-freezing in liquid nitrogen for data collection. Diffraction data were collected at the Diamond Light Source. The best diffracting crystals grew under the conditions described in **Table 1**. When noted, crystal optimization used Newman's buffer system(Newman 2004) and defined PEG smears (Chaikuad, Knapp et al. 2015).

Structure Solution and Refinement. Diffraction data were integrated using XDS (Kabsch 2010) and scaled using AIMLESS from the CCP4 software suite (Winn, Ballard et al. 2011). Molecular replacement for was performed with Phaser (McCoy, Grosse-Kunstleve et al. 2007) using BIKE/AZD7762 (PDB ID: 4W9W) (Sorrell, Szklarz et al. 2016) as a search model. Automated model building was performed with Buccanner (Cowtan 2006). Automated refinement was performed in PHENIX (Zhang, Cowtan et al. 1997). Coot (Emsley, Lohkamp et al. 2010) was used for manual model building and

bioRxiv preprint doi: https://doi.org/10.1101/094631; this version posted December 15, 2016. The copyright holder for this preprint (which was not certified by peer review) is the author/funder, who has granted bioRxiv a license to display the preprint in perpetuity. It is made available under aCC-BY 4.0 International license.

refinement. Structure validation was performed using MolProbity (Chen, Arendall et al. 2010). Structure factors and coordinates have been deposited in the PDB (see Table 1).

Computation. Solvation free energies and quantum mechanical calculations were run using Macromodel (Schrödinger Release 2016-3: MacroModel, Schrödinger, LLC New York, NY, 2016.) and Jaguar Schrödinger Release 2016-4: Jaguar, Schrödinger, LLC, New York, NY, 2016. from Schrodinger Inc.

ACKNOWLEDGMENT

Aled Edwards is acknowledged for illuminating discussions and encouragement in the preparation of this manuscript. We thank Diamond Light Source for access to beamline I03 (proposal number MX14664) that contributed to the results presented here. The SGC is a registered charity (number 1097737) that receives funds from AbbVie, Bayer Pharma AG, Boehringer Ingelheim, Canada Foundation for Innovation, Eshelman Institute for Innovation, Genome Canada, Innovative Medicines Initiative (EU/EFPIA), Janssen, Merck & Co., Novartis Pharma AG, Ontario Ministry of Economic Development and Innovation, Pfizer, São Paulo Research Foundation-FAPESP, Takeda, and Wellcome Trust.

bioRxiv preprint doi: https://doi.org/10.1101/094631; this version posted December 15, 2016. The copyright holder for this preprint (which was not certified by peer review) is the author/funder, who has granted bioRxiv a license to display the preprint in perpetuity. It is made available under aCC-BY 4.0 International license.

Table 1. K_d values for selected kinases. K_d values were determined for kinases observed to have >70% displacement of immobilized ligand with either **1** or **2** in a KINOMEscan screen at 1 µM compound.

Kinase	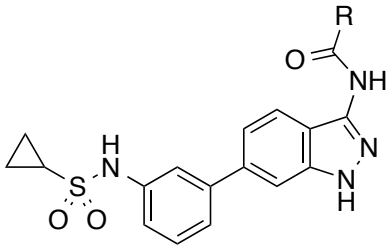		**K_d Ratio 2:1**
	1 (R = cyclopropyl) K_d (nM)	**2** (R = *i*-Pr) K_d (nM)	
AAK1	71	8800	124
BIKE	68	>10000	>150
BRAF	100	52	0.52
RIOK1	170	9600	56
PDGFRB	250	61	0.24
KIT	290	77	0.27
RIOK3	300	8200	27
DDR1	400	150	0.38
ABL1	540	190	0.35
RAF1	580	350	0.60
PDGFRA	590	240	0.41
CSF1R	2000	1600	0.80
p38a	6900	550	0.08

bioRxiv preprint doi: https://doi.org/10.1101/094631; this version posted December 15, 2016. The copyright holder for this preprint (which was not certified by peer review) is the author/funder, who has granted bioRxiv a license to display the preprint in perpetuity. It is made available under aCC-BY 4.0 International license.

Table 2. NAK family FRET-based binding displacement assay results.

Kinase	K_i (nM)		Ratio
	1	**2**	
AAK1	8.3	2700	320
BIKE	13	3100	240
GAK	1600	4900	3
STK16	330	19000	58

bioRxiv preprint doi: https://doi.org/10.1101/094631; this version posted December 15, 2016. The copyright holder for this preprint (which was not certified by peer review) is the author/funder, who has granted bioRxiv a license to display the preprint in perpetuity. It is made available under aCC-BY 4.0 International license.

Table 3. Crystal structure data collection and refinement statistics.

Protein	BIKE
Ligand	**1**
X-ray source	DLS I02
a (Å)	41.96
b (Å)	111.15
c (Å)	164.05
α, β, γ (°)	90, 90, 90
Space group	I 2 2 2
Wavelength (Å)	0.97949
Resolution limit (Å)*	28.6-2.41 (2.50-2.41)
Number of observations*	81.078 (7,855)
Completeness (%)*	99.1 (95.2)
Multiplicity*	5.3 (5.2)
Rmerge (%)*	0.074 (0.49)
Mean I/σI *	13.2 (3.1)
Refinement	
Resolution Range (Å)	21.75-2.41
Rcryst	0.176
Rfree	0.216
No. protein atoms	2,317
No. ligand atoms	28
No. solvent atoms	89
Mean B-factor (Å)	53.1
Rmsd bond lengths (Å)	0.010
Rmsd bond angles (°)	1.04
Ramachandran statistics (%)	
Favored	98.3
Allowed	1.7
Outlier	0
PDB ID	5IKW
Crystallization conditions	10% (v/v) Broad MW PEG smear, 3.2 M $MgCl_2$, 100 mM Hepes pH 7.0

* Highest resolution shell shown in parentheses

bioRxiv preprint doi: https://doi.org/10.1101/094631; this version posted December 15, 2016. The copyright holder for this preprint (which was not certified by peer review) is the author/funder, who has granted bioRxiv a license to display the preprint in perpetuity. It is made available under aCC-BY 4.0 International license.

Table 4. Previously reported matched pairs of kinase inhibitors demonstrating an affinity or activity cliff between cyclopropyl and isopropyl compounds.

Structure	Activity
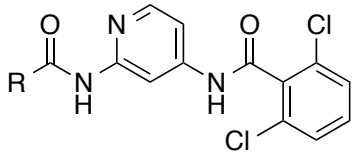 **3**	TYK2 K_i **3a** = Cyclopropyl: 4.8 nM **3b** = Isopropyl: 840 nM Ref: (Liang, Tsui et al. 2013)
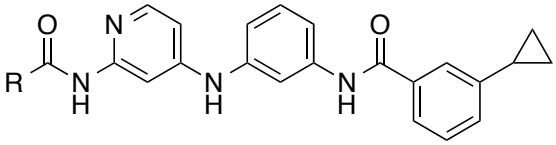 **4**	B-Raf^{V600E} IC_{50} **4a**: R = Cyclopropyl: 35 nM **4b**: R = Isopropyl: 420 nM Ref: (Li, Shen et al. 2016)

bioRxiv preprint doi: https://doi.org/10.1101/094631; this version posted December 15, 2016. The copyright holder for this preprint (which was not certified by peer review) is the author/funder, who has granted bioRxiv a license to display the preprint in perpetuity. It is made available under aCC-BY 4.0 International license.

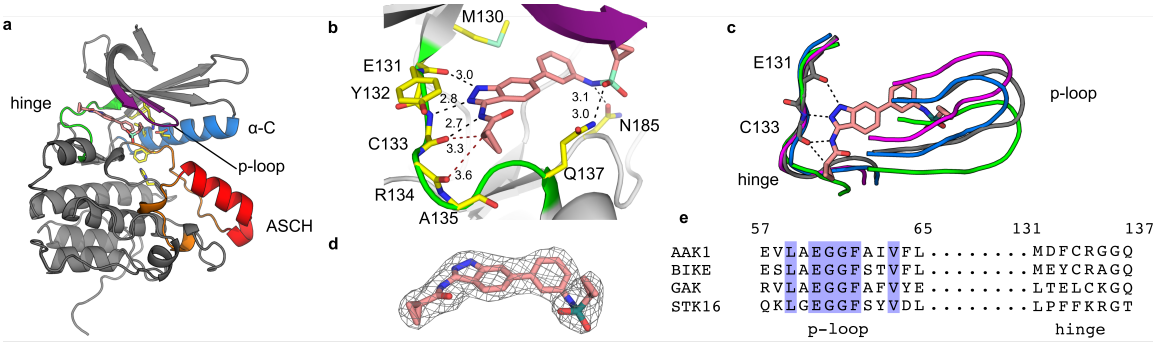

Figure 1. Crystallographic characterization of BIKE bound to 3-acylaminoindazole **1**. (**a)** BIKE-**1** adopts an active conformation. Protein (cartoon) regions important for activity and ligand interaction are indicated and highlighted in different colors. As for other NAK-family members, the activation segment of BIKE (orange) contains a C-terminal helical segment (ASCH; in red). Inhibitor **1** (carbon atoms in pink) and BIKE residues (carbon atoms in yellow) taking part in the regulatory hydrophobic spine and the critical ion pair leading to an active conformation are shown as sticks. (**b**) Details of the BIKE-**1** interactions. Inhibitor **1** is anchored to the hinge (green ribbon) via hydrogen bonds (dashed lines) and complements the hydrophobic cavity formed by aliphatic side chains from p-loop (purple ribbon) and β-6 residues. Potential interactions between main chain carbonyl and the cyclopropane group are indicated by dashed lines. Hydrogen bonds between Asn185, Gln137 and the sulfonamide group are also shown (dashed lines). (**c**) Superposition of NAK family proteins AAK1 (blue; PDB ID 4WSQ), BIKE (grey, PDB IDs 5IKW, this work), GAK (PDB ID 4Y8D) and MPSK1 (PDB ID 2BUJ) shows variation in the p-loop region despite good alignment in the hinge region. Compound anchoring hydrogen bonds are shown for BIKE and **1** (sticks). (**d**) Electron density (2Fo-Fc) maps (grey mash; 1.0 σ contour) for **1**. (**e**) Primary sequence comparison of NAK family hinge and P-loop regions.

bioRxiv preprint doi: https://doi.org/10.1101/094631; this version posted December 15, 2016. The copyright holder for this preprint (which was not certified by peer review) is the author/funder, who has granted bioRxiv a license to display the preprint in perpetuity. It is made available under aCC-BY 4.0 International license.

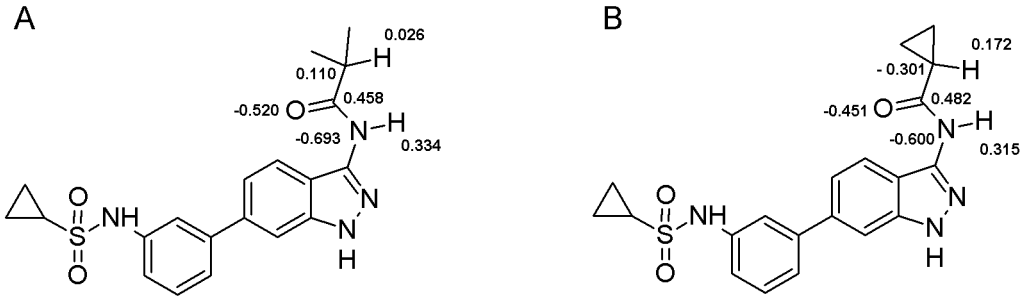

Figure 2. Computationally generated electrostatic potential (ESP) derived atomic charges for (A) **1** and (B) **2**.

bioRxiv preprint doi: https://doi.org/10.1101/094631; this version posted December 15, 2016. The copyright holder for this preprint (which was not certified by peer review) is the author/funder, who has granted bioRxiv a license to display the preprint in perpetuity. It is made available under aCC-BY 4.0 International license.

A

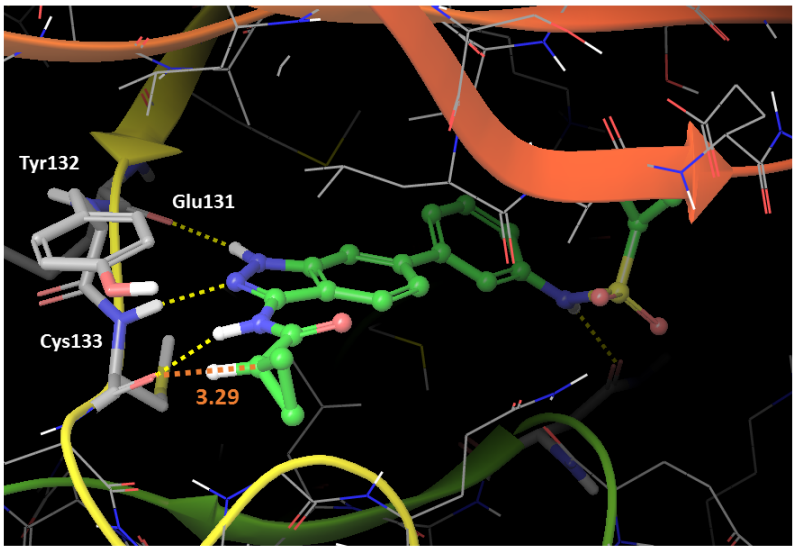

B

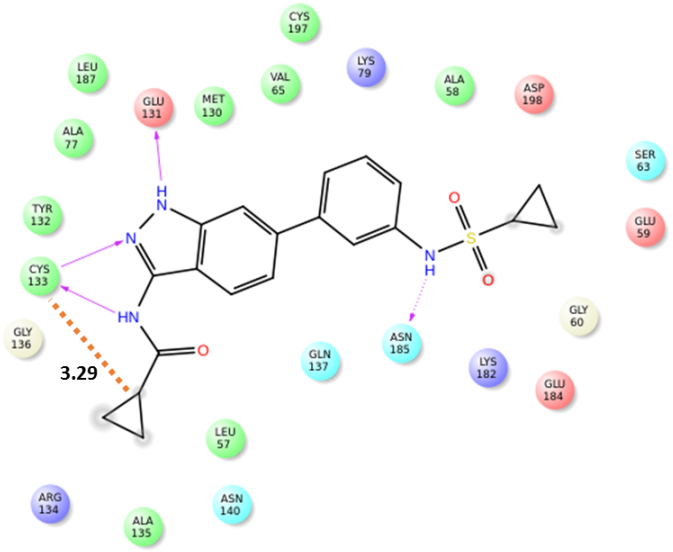

Figure 3. (A) **1** bound in BIKE active site. (B) Two dimensional compound interaction diagram of **1** and BIKE depicting adjacent residues and key interactions.

bioRxiv preprint doi: https://doi.org/10.1101/094631; this version posted December 15, 2016. The copyright holder for this preprint (which was not certified by peer review) is the author/funder, who has granted bioRxiv a license to display the preprint in perpetuity. It is made available under aCC-BY 4.0 International license.

REFERENCES

Arrowsmith, C. H., J. E. Audia, C. Austin, J. Baell, J. Bennett, J. Blagg, C. Bountra, P. E. Brennan, P. J. Brown, M. E. Bunnage, C. Buser-Doepner, R. M. Campbell, A. J. Carter, P. Cohen, R. A. Copeland, B. Cravatt, J. L. Dahlin, D. Dhanak, A. M. Edwards, M. Frederiksen, S. V. Frye, N. Gray, C. E. Grimshaw, D. Hepworth, T. Howe, K. V. Huber, J. Jin, S. Knapp, J. D. Kotz, R. G. Kruger, D. Lowe, M. M. Mader, B. Marsden, A. Mueller-Fahrnow, S. Muller, R. C. O'Hagan, J. P. Overington, D. R. Owen, S. H. Rosenberg, B. Roth, R. Ross, M. Schapira, S. L. Schreiber, B. Shoichet, M. Sundstrom, G. Superti-Furga, J. Taunton, L. Toledo-Sherman, C. Walpole, M. A. Walters, T. M. Willson, P. Workman, R. N. Young and W. J. Zuercher (2015). "The promise and peril of chemical probes." Nat Chem Biol **11**(8): 536-541.

Chaikuad, A., T. Keates, C. Vincke, M. Kaufholz, M. Zenn, B. Zimmermann, C. Gutierrez, R. G. Zhang, C. Hatzos-Skintges, A. Joachimiak, S. Muyldermans, F. W. Herberg, S. Knapp and S. Muller (2014). "Structure of cyclin G-associated kinase (GAK) trapped in different conformations using nanobodies." Biochem J **459**(1): 59-69.

Chaikuad, A., S. Knapp and F. von Delft (2015). "Defined PEG smears as an alternative approach to enhance the search for crystallization conditions and crystal-quality improvement in reduced screens." Acta Crystallogr D Biol Crystallogr **71**(Pt 8): 1627-1639.

Chen, V. B., W. B. Arendall, 3rd, J. J. Headd, D. A. Keedy, R. M. Immormino, G. J. Kapral, L. W. Murray, J. S. Richardson and D. C. Richardson (2010). "MolProbity: all-atom structure validation for macromolecular crystallography." Acta Crystallogr D Biol Crystallogr **66**(Pt 1): 12-21.

Cohen, P. and D. R. Alessi (2013). "Kinase drug discovery--what's next in the field?" ACS Chem Biol **8**(1): 96-104.

Cowtan, K. (2006). "The Buccaneer software for automated model building. 1. Tracing protein chains." Acta Crystallogr D Biol Crystallogr **62**(Pt 9): 1002-1011.

Davis, M. I., J. P. Hunt, S. Herrgard, P. Ciceri, L. M. Wodicka, G. Pallares, M. Hocker, D. K. Treiber and P. P. Zarrinkar (2011). "Comprehensive analysis of kinase inhibitor selectivity." Nat Biotechnol **29**(11): 1046-1051.

Derewenda, Z. S. (2004). "Rational protein crystallization by mutational surface engineering." Structure **12**(4): 529-535.

Emsley, P., B. Lohkamp, W. G. Scott and K. Cowtan (2010). "Features and development of Coot." Acta Crystallogr D Biol Crystallogr **66**(Pt 4): 486-501.

Eswaran, J., A. Bernad, J. M. Ligos, B. Guinea, J. E. Debreczeni, F. Sobott, S. A. Parker, R. Najmanovich, B. E. Turk and S. Knapp (2008). "Structure of the human protein kinase MPSK1 reveals an atypical activation loop architecture." Structure **16**(1): 115-124.

Fabian, M. A., W. H. Biggs, 3rd, D. K. Treiber, C. E. Atteridge, M. D. Azimioara, M. G. Benedetti, T. A. Carter, P. Ciceri, P. T. Edeen, M. Floyd, J. M. Ford, M. Galvin, J. L. Gerlach, R. M. Grotzfeld, S. Herrgard, D. E. Insko, M. A. Insko, A. G. Lai, J. M. Lelias, S. A. Mehta, Z. V. Milanov, A. M. Velasco, L. M. Wodicka, H. K. Patel, P. P. Zarrinkar and D. J. Lockhart (2005). "A small molecule-kinase interaction map for clinical kinase inhibitors." Nat Biotechnol **23**(3): 329-336.

bioRxiv preprint doi: https://doi.org/10.1101/094631; this version posted December 15, 2016. The copyright holder for this preprint (which was not certified by peer review) is the author/funder, who has granted bioRxiv a license to display the preprint in perpetuity. It is made available under aCC-BY 4.0 International license.

Fedorov, O., S. Muller and S. Knapp (2010). "The (un)targeted cancer kinome." Nat Chem Biol **6**(3): 166-169.

Frisch, M. J., J. A. Pople and J. S. Binkley (1984). J. Chem. Phys.: 3265.

Galano, A., J. Alvarez-Idaboy and A. Vivier-Bunge (2007). "Non-alkane behavior of cyclopropane and its derivatives: characterization of unconventional hydrogen bond interactions." Theor. Chem. Account **118**: 597-606.

Harder, E., W. Damm, J. Maple, C. Wu, M. Reboul, J. Y. Xiang, L. Wang, D. Lupyan, M. K. Dahlgren, J. L. Knight, J. W. Kaus, D. S. Cerutti, G. Krilov, W. L. Jorgensen, R. Abel and R. A. Friesner (2016). "OPLS3: A Force Field Providing Broad Coverage of Drug-like Small Molecules and Proteins." J Chem Theory Comput **12**(1): 281-296.

Huse, M. and J. Kuriyan (2002). "The conformational plasticity of protein kinases." Cell **109**(3): 275-282.

Kabsch, W. (2010). "Xds." Acta Crystallogr D Biol Crystallogr **66**(Pt 2): 125-132.

Knapp, S., P. Arruda, J. Blagg, S. Burley, D. H. Drewry, A. Edwards, D. Fabbro, P. Gillespie, N. S. Gray, B. Kuster, K. E. Lackey, P. Mazzafera, N. C. Tomkinson, T. M. Willson, P. Workman and W. J. Zuercher (2013). "A public-private partnership to unlock the untargeted kinome." Nat Chem Biol **9**(1): 3-6.

Kornev, A. P. and S. S. Taylor (2010). "Defining the conserved internal architecture of a protein kinase." Biochim Biophys Acta **1804**(3): 440-444.

Lebakken, C. S., S. M. Riddle, U. Singh, W. J. Frazee, H. C. Eliason, Y. Gao, L. J. Reichling, B. D. Marks and K. W. Vogel (2009). "Development and applications of a broad-coverage, TR-FRET-based kinase binding assay platform." J Biomol Screen **14**(8): 924-935.

Li, X., J. Shen, L. Tan, Z. Zhang, D. Gao, J. Luo, H. Cheng, X. Zhou, J. Ma, K. Ding and X. Lu (2016). "Design and synthesis of N-(4-aminopyridin-2-yl)amides as B-Raf(V600E) inhibitors." Bioorg Med Chem Lett **26**(12): 2760-2763.

Liang, J., V. Tsui, A. Van Abbema, L. Bao, K. Barrett, M. Beresini, L. Berezhkovskiy, W. S. Blair, C. Chang, J. Driscoll, C. Eigenbrot, N. Ghilardi, P. Gibbons, J. Halladay, A. Johnson, P. B. Kohli, Y. Lai, M. Liimatta, P. Mantik, K. Menghrajani, J. Murray, A. Sambrone, Y. Xiao, S. Shia, Y. Shin, J. Smith, S. Sohn, M. Stanley, M. Ultsch, B. Zhang, L. C. Wu and S. Magnuson (2013). "Lead identification of novel and selective TYK2 inhibitors." Eur J Med Chem **67**: 175-187.

Liu, H. P., Y. J. Lin, W. Y. Lin, L. Wan, J. J. Sheu, H. J. Lin, Y. Tsai, C. H. Tsai and F. J. Tsai (2009). "A novel genetic variant of BMP2K contributes to high myopia." J Clin Lab Anal **23**(6): 362-367.

McCoy, A. J., R. W. Grosse-Kunstleve, P. D. Adams, M. D. Winn, L. C. Storoni and R. J. Read (2007). "Phaser crystallographic software." J Appl Crystallogr **40**(Pt 4): 658-674.

Neveu, G., A. Ziv-Av, R. Barouch-Bentov, E. Berkerman, J. Mulholland and S. Einav (2015). "AP-2-associated protein kinase 1 and cyclin G-associated kinase regulate hepatitis C virus entry and are potential drug targets." J Virol **89**(8): 4387-4404.

Newman, J. (2004). "Novel buffer systems for macromolecular crystallization." Acta Crystallogr D Biol Crystallogr **60**(Pt 3): 610-612.

Ruegg, U. T. and G. M. Burgess (1989). "Staurosporine, K-252 and UCN-01: potent but nonspecific inhibitors of protein kinases." Trends Pharmacol Sci **10**(6): 218-220.

bioRxiv preprint doi: https://doi.org/10.1101/094631; this version posted December 15, 2016. The copyright holder for this preprint (which was not certified by peer review) is the author/funder, who has granted bioRxiv a license to display the preprint in perpetuity. It is made available under aCC-BY 4.0 International license.

Sakurai, M. A., Y. Ozaki, D. Okuzaki, Y. Naito, T. Sasakura, A. Okamoto, H. Tabara, T. Inoue, M. Hagiyama, A. Ito, N. Yabuta and H. Nojima (2014). "Gefitinib and luteolin cause growth arrest of human prostate cancer PC-3 cells via inhibition of cyclin G-associated kinase and induction of miR-630." PLoS One **9**(6): e100124.

Shi, B., S. D. Conner and J. Liu (2014). "Dysfunction of endocytic kinase AAK1 in ALS." Int J Mol Sci **15**(12): 22918-22932.

Sorrell, F. J., M. Szklarz, K. R. Abdul Azeez, J. M. Elkins and S. Knapp (2016). "Family-wide Structural Analysis of Human Numb-Associated Protein Kinases." Structure **24**(3): 401-411.

Stephens, P. J., F. J. Devlin, C. F. Chabalowski and M. J. Frisch (1994). J. Phys. Chem. **98**: 11623.

Still, W. C., A. Tempczyk, R. C. Hawley and T. Hendrickson (1990). "Semianalytical Treatment of Solvation for Molecular Mechanics and Dynamics." J. Am. Chem. Soc. **112**: 6127-6129.

Stumpfe, D. and J. Bajorath (2012). "Exploring activity cliffs in medicinal chemistry." J Med Chem **55**(7): 2932-2942.

Talele, T. T. (2016). "The "Cyclopropyl Fragment" is a Versatile Player that Frequently Appears in Preclinical/Clinical Drug Molecules." J Med Chem **59**(19): 8712-8756.

Uitdehaag, J. C., F. Verkaar, H. Alwan, J. de Man, R. C. Buijsman and G. J. Zaman (2012). "A guide to picking the most selective kinase inhibitor tool compounds for pharmacological validation of drug targets." Br J Pharmacol **166**(3): 858-876.

Winn, M. D., C. C. Ballard, K. D. Cowtan, E. J. Dodson, P. Emsley, P. R. Evans, R. M. Keegan, E. B. Krissinel, A. G. Leslie, A. McCoy, S. J. McNicholas, G. N. Murshudov, N. S. Pannu, E. A. Potterton, H. R. Powell, R. J. Read, A. Vagin and K. S. Wilson (2011). "Overview of the CCP4 suite and current developments." Acta Crystallogr D Biol Crystallogr **67**(Pt 4): 235-242.

Witherington, J., V. Bordas, A. Gaiba, A. Naylor, A. D. Rawlings, B. P. Slingsby, D. G. Smith, A. K. Takle and R. W. Ward (2003). "6-heteroaryl-pyrazolo[3,4-b]pyridines: potent and selective inhibitors of glycogen synthase kinase-3 (GSK-3)." Bioorg Med Chem Lett **13**(18): 3059-3062.

Xing, L., J. Klug-Mcleod, B. Rai and E. A. Lunney (2015). "Kinase hinge binding scaffolds and their hydrogen bond patterns." Bioorg Med Chem **23**(19): 6520-6527.

Zhang, K. Y., K. Cowtan and P. Main (1997). "Combining constraints for electron-density modification." Methods Enzymol **277**: 53-64.